

SubspaceNet: Deep Learning-Aided Subspace Methods for DoA Estimation

Dor H. Shmuel, Julian P. Merkofer, Guy Revach, Ruud J. G. van Sloun, and Nir Shlezinger

Abstract—Direction of arrival (DoA) estimation is a fundamental task in array processing. A popular family of DoA estimation algorithms are subspace methods, which operate by dividing the measurements into distinct signal and noise subspaces. Subspace methods, such as Multiple Signal Classification (MUSIC) and Root-MUSIC, rely on several restrictive assumptions, including narrowband non-coherent sources and fully calibrated arrays, and their performance is considerably degraded when these do not hold. In this work we propose SubspaceNet; a data-driven DoA estimator which learns how to divide the observations into distinguishable subspaces. This is achieved by utilizing a dedicated deep neural network to learn the empirical autocorrelation of the input, by training it as part of the Root-MUSIC method, leveraging the inherent differentiability of this specific DoA estimator, while removing the need to provide a ground-truth decomposable autocorrelation matrix. Once trained, the resulting SubspaceNet serves as a universal surrogate covariance estimator that can be applied in combination with any subspace-based DoA estimation method, allowing its successful application in challenging setups. SubspaceNet is shown to enable various DoA estimation algorithms to cope with coherent sources, wideband signals, low SNR, array mismatches, and limited snapshots, while preserving the interpretability and the suitability of classic subspace methods.

I. INTRODUCTION

Direction of arrival (DoA) estimation is a common array processing task, which deals with localizing emitting sources by determining the incidence angles of impinging waves [2]. A leading and well-trusted family of DoA estimators is based on *subspace methods*, including the celebrated Multiple Signal Classification (MUSIC) algorithm [3], Root-MUSIC (Root-MUSIC) [4], and Estimation of Signal Parameters via Rotational Invariance Techniques (ESPRIT) [5]. When given sufficient signal snapshots, these techniques estimate multiple DoAs with low complexity by separating the impinging wave into distinguishable signal and noise subspaces, achieving angular resolution that is not limited by the array geometry [2].

The ability to separate an impinging wave into signal and noise subspaces, which is the core of subspace methods, relies on the orthogonality between the noise components and the array response. For this to hold, several key requirements must be satisfied: the signals need to be narrowband and non-coherent; the array has to be fully calibrated; sufficient snapshots are needed to estimate the covariance; and the

statistical model underlying the estimation procedure has to be fully known. As these requirements are often violated in practical settings, different pre-processing methods such as the spatial smoothing (SPS) and FB, have been proposed to tackle some of these limitations individually, e.g., [6], [7]. These schemes average the power spectrum of the received signals over a number of adjacent sensor positions, thereby increasing the effective aperture, while resulting in a trade-off between resolution and variance reduction. Specifically, larger averaging windows results in better variance reduction but poorer resolution, while smaller windows result in better resolution but poorer variance reduction. Hence, they tend to degrade the overall estimation performance and resolution, while constraining the number of recoverable sources.

Over the last decade, deep learning has emerged as a leading tool for data-driven inference. Deep neural networks (DNNs), which learn their mapping from data without relying on system modelling, have demonstrated unprecedented success in areas involving complex data such as computer vision [8]. Accordingly, DNN-based approaches have recently been considered for DoA estimation [9]–[21], as also surveyed in [22]. Specifically, in [9]–[14] different DNN architectures such as multi-layer perceptrons (MLPs) [9], convolutional neural networks (CNNs) [10]–[13], and ResNet variants [14], were trained to learn the mapping from the observations or their empirical covariance directly into DoAs. While DNNs can be trained to estimate DoAs without imposing specific requirements on the signal model, they typically require highly parameterized architectures trained with massive data sets, limiting their applicability on hardware-limited devices where DoA estimation is often carried out. Furthermore, black-box DNNs lack the interpretability and flexibility of model-based algorithms, and often give rise to generalization issues.

An alternative approach uses DNNs alongside model-based DoA estimation, as a form of model-based deep learning [23], [24]. For instance, the work [15] reduced the complexity of maximum likelihood DoA recovery by using a DNN to limit the angular search space, thus still relying on accurate statistical modelling of the signals. The work [16] used narrowband signal modelling to train CNN-based DoA estimators in an unsupervised manner. In the context of subspace methods, [17] trained an autoencoder to reconstruct a clean input from a corrupted and then pass it to MLP classifiers to reconstruct a MUSIC spectrum, while [18]–[20] used DNNs to directly produce a (discretized) spatial spectrum. However, these DNN-aided estimators [17]–[20] were not trained to provide DoAs, and share the limitations of model-based subspace methods. The work [21] proposed an architecture that jointly learns to

Parts of this work were accepted for presentation in the 2023 IEEE International Conference on Acoustics Speech, and Signal Processing (ICASSP) as the paper [1]. D. H. Shmuel and N. Shlezinger are with the School of ECE, Ben-Gurion University of the Negev, Beer Sheva, Israel (e-mail: shmueldo@post.bgu.ac.il; nirshl@bgu.ac.il). J. P. Merkofer and R. J. G. van Sloun are with the EE Dpt., Eindhoven University of Technology, The Netherlands (e-mail: {j.p.merkofer; r.j.g.v.sloun}@tue.nl). G. Revach is with the D-ITET, ETH Zürich, Switzerland, (email: grevach@ethz.ch).

compute the empirical covariance along with the processing of the resulting MUSIC spectrum. The resulting estimator was capable of coping with coherent and wideband sources. However, this came at the cost of compromising on the interpretability of subspace methods, as the DoAs were recovered from the empirical covariance using an additional DNN, learning a deep model where one cannot extract meaningful interpretation from its MUSIC spectrum. This motivates designing DNN-aided DoA estimators that cope with the limitations of model-based subspace methods, e.g., coherent sources and few snapshots, while preserving their interpretability and suitability.

Here, we propose *SubspaceNet*, which leverages data to implement subspace-based DoA estimation. SubspaceNet is designed to cope with coherent sources, broadband signals, few snapshots, and calibration mismatches. This is achieved by identifying that these limitations of model-based subspace methods are encapsulated in their reliance on the empirical covariance of the received signals. SubspaceNet thus preserves the operation of subspace methods while using a dedicated trainable autoencoder which learns from data how to map the empirical auto-correlation of the observed signal into a surrogate covariance that is universally useful for subspace-based DoA recovery, i.e., that is decomposable into signal and noise subspaces.

In order to train an autoencoder that produces subspace-compliant covariance estimates, we exploit the inherent differentiability of Root-MUSIC to convert the algorithm into a trainable discriminative model [25]. By doing so, the trained DNN computes meaningful subspace representations leading to accurate DoA estimates, without having to provide ground-truth decomposable covariances. SubspaceNet thus learns to compute meaningful subspace representations that, once trained, can be combined with different subspace DoA estimators, including MUSIC, Root-MUSIC, and ESPRIT. We empirically show that SubspaceNet outperforms model-based subspace methods for both coherent and non-coherent sources, and that it successfully operates with broadband signals, calibration mismatches, low signal-to-noise ratio (SNR), and few snapshots. We also demonstrate the SubspaceNet creates a clear and significant distinction between the noise and the signal subspaces, which facilitates its diagnosis and identifying of the number of sources.

The rest of the paper is organized as follows: Section II formulates the setup and recalls subspace methods. Section III presents SubspaceNet, which is numerically evaluated in Section IV. Finally, Section V concludes the paper.

Throughout this paper, we use boldface-uppercase for matrices, e.g., \mathbf{X} , boldface-lowercase for vectors, e.g., \mathbf{x} . We denote the j th entry of vector \mathbf{x} and the (i, j) th entry of matrix \mathbf{X} by $[x]_j$ and $[\mathbf{X}]_{i,j}$, respectively. We use $(\cdot)^H$, $(\cdot)^T$, $\|\cdot\|$, and $\mathbb{E}[\cdot]$ for the hermitian transpose, transpose, ℓ_2 norm, and stochastic expectation, respectively.

II. SYSTEM MODEL AND PRELIMINARIES

In this section, we present the system model, beginning with received signal model in Subsection II-A. We then briefly review subspace-based DoA estimation in Subsection II-B, and formulate the considered problem in Subsection II-C.

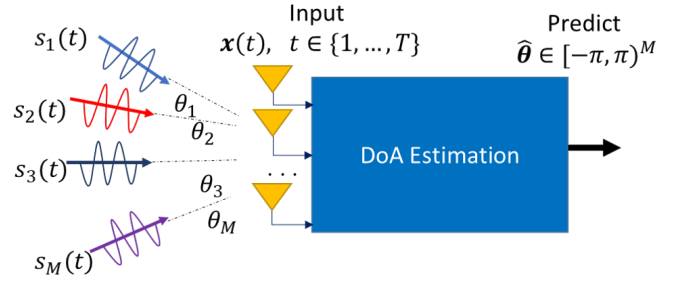


Fig. 1: DoA estimation system illustration.

A. DoA Estimation Signal Model

We consider a receiver equipped with a uniform linear array (ULA) composed of N half-wavelength spaced antenna elements. At each discrete time instance t (out of a horizon of T snapshots, i.e., $t \in \{1, \dots, T\}$), the receiver gathers multidimensional observations, denoted $\mathbf{x}(t) = [x_1(t), \dots, x_N(t)] \in \mathbb{C}^N$. These signals originate from M sources, represented as $\mathbf{s}(t) = [s_1(t), \dots, s_M(t)] \in \mathbb{C}^M$, and the DoAs of these sources are denoted in vector form as $\boldsymbol{\theta} = [\theta_1, \dots, \theta_M]$. The system is illustrated in Fig. 1. *DoA estimation* is the recovery of $\boldsymbol{\theta}$ from the observations obtained over T snapshots.

When the transmitted signals are narrowband and in the far-field of the array, the received signal over T snapshots, denoted $\mathbf{X} = [\mathbf{x}(1), \dots, \mathbf{x}(T)] \in \mathbb{C}^{N \times T}$ is typically modelled as

$$\mathbf{X} = \mathbf{A}(\boldsymbol{\theta})\mathbf{S} + \mathbf{V}. \quad (1)$$

In (1), $\mathbf{S} = [s(1), \dots, s(T)] \in \mathbb{C}^{M \times T}$ is the sources signals matrix; $\mathbf{V} \in \mathbb{C}^{N \times T}$ is the noise matrix comprised of i.i.d. entries with variance σ_V^2 ; and $\mathbf{A}(\boldsymbol{\theta}) = [\mathbf{a}(\theta_1), \dots, \mathbf{a}(\theta_M)] \in \mathbb{C}^{N \times M}$ is the steering matrix, where

$$\mathbf{a}(\theta) \triangleq [1, e^{-j\pi \sin(\theta)}, \dots, e^{-j\pi(N-1)\sin(\theta)}]. \quad (2)$$

When the sources are zero-mean and stationary, the covariance of the observations is obtained from (1) as

$$\mathbf{R}_X = \mathbb{E}[\mathbf{X}\mathbf{X}^H] = \mathbf{A}(\boldsymbol{\theta})\mathbf{R}_S\mathbf{A}^H(\boldsymbol{\theta}) + \sigma_V^2\mathbf{I}_N, \quad (3)$$

where \mathbf{R}_S denotes the covariance of \mathbf{S} .

B. Subspace-Based DoA Estimation

Subspace methods are a family of DoA estimation algorithms that rely on the ability to decompose the observations covariance matrix in (3) into orthogonal signal and noise subspaces. They are based on the following assumptions:

- AS1 The sources are narrowband, such that (1) holds.
- AS2 The sources are non-coherent, namely, the covariance matrix \mathbf{R}_S in (3) is diagonal.
- AS3 The array is calibrated, such that the steering vectors in (2) are known and accurately match the array.
- AS4 The number of snapshots T is sufficiently large, and the SNR is sufficiently high, such that one can reliably estimate \mathbf{R}_X in (3) empirically as

$$\hat{\mathbf{R}}_X = \frac{1}{T}\mathbf{X}\mathbf{X}^H. \quad (4)$$

Under assumptions AS1-AS3, subspace methods decompose the covariance matrix \mathbf{R}_X in (3), which can be sufficiently estimated under AS4, into orthogonal subspaces. To

see this, we write the eigenvalue decomposition (EVD) of \mathbf{R}_X as

$$\mathbf{R}_X = \mathbf{U}\mathbf{\Lambda}\mathbf{U}^H, \quad (5)$$

where $\mathbf{\Lambda}$ is the diagonal eigenvalues matrix while the unitary matrix $\mathbf{U} = [\mathbf{u}_1, \dots, \mathbf{u}_N]$ is their corresponding eigenvectors. The resulting eigenvectors \mathbf{U} span an observation space that can be divided into two orthogonal subspaces: the signal subspace \mathbf{U}_S and the noise subspace \mathbf{U}_N [3], i.e.,

$$\mathbf{U} = [\mathbf{U}_S | \mathbf{U}_N], \quad \text{where } \mathbf{U}_S \perp \mathbf{U}_N. \quad (6)$$

In (6), \mathbf{U}_S contains M eigenvectors, each corresponding to a specific directional impinging source [26], and is spanned by the columns of the steering matrix $\mathbf{A}(\theta)$; the $(N - M) \times N$ matrix \mathbf{U}_N , comprised of the eigenvectors corresponding to the $N - M$ least dominant eigenvalues of \mathbf{R}_X (which equal σ_V^2), represents the noise subspace.

The representation (6) implies that $\mathbf{A}(\theta) \perp \mathbf{U}_N$, leading to

$$\mathbf{a}^H(\theta_i) \mathbf{U}_N \mathbf{U}_N^H \mathbf{a}(\theta_i) = \|\mathbf{U}_N^H \mathbf{a}(\theta_i)\|^2 = 0, \quad (7)$$

for all $i \in 1, \dots, M$. Equation (7) forms the basis of subspace methods, which use it to identify the DoAs, as reviewed next.

1) *MUSIC*: Arguably the most common subspace-based DoA estimator is MUSIC [3]. Here, (7) is used to construct a spectrum representation by taking the inverse projection of the steering vectors on the noise subspace. In particular, the noise subspace matrix and the number of sources are estimated from the EVD of the empirical covariance (4) as \hat{M} and $\hat{\mathbf{U}}_N$, respectively. The resulting MUSIC spectrum is given by

$$P_{\text{MUSIC}}(\theta) = \frac{1}{\|\hat{\mathbf{U}}_N^H \mathbf{a}(\theta)\|^2}. \quad (8)$$

The DoAs are then recovered by identifying the peaks of the constructed spectrum $P_{\text{MUSIC}}(\theta)$, i.e., the MUSIC spectrum provides an interpretable visual representation of the DoAs.

2) *Root-MUSIC*: An alternative approach to recover the DoAs from the estimated $\hat{\mathbf{U}}_N$ seeks the roots of (7). In particular, Root-MUSIC formulates the Hermitian matrix $\mathbf{F} = \hat{\mathbf{U}}_N \hat{\mathbf{U}}_N^H$ using its diagonal sum coefficients f_n , defined as

$$f_n = \sum_{i=0}^{N-1-n} [\mathbf{F}]_{i, n+i}, \quad n \geq 0, \quad (9)$$

where for $n < 0$, $f_n = f_{|n|}^*$. Substituting (9) into (7), the left hand side of (7) can be expressed as a polynomial equation in a complex-valued argument z of order $2N - 2$, given by

$$\begin{aligned} D(z) &= \sum_{i=0}^{N-1} \sum_{j=0}^{N-1} [\mathbf{a}(\theta)]_i^* [\mathbf{F}]_{ij} [\mathbf{a}(\theta)]_j \\ &= \sum_{i=0}^{N-1} \sum_{j=0}^{N-1} [\mathbf{F}]_{ij} z^{i-j} = \sum_{n=-(N-1)}^{N-1} f_n z^n, \end{aligned} \quad (10)$$

where $z = e^{-j\pi \sin(\theta)}$. Root-MUSIC identifies the DoAs from the roots of the polynomial (10). The roots map is viewed as the Root-MUSIC spectrum. Since (10) has $2N - 2 > M$ roots (divided into symmetric pairs), while the roots corresponding to DoAs should have unit magnitude, the \hat{M} pairs of roots

which are the closest to the unit circle are matched as the \hat{M} sources DoAs [4]. Similarly to MUSIC, the Root-MUSIC spectrum provides a meaningful visualization of the DoAs.

3) *ESPRIT*: The popular ESPRIT subspace method separates the array into two overlapping sub-arrays, where it exploits the rotational invariance of the covariance matrix eigenstructure to simplify DoA estimation [5]. The steering matrices of the subarrays are related by $\mathbf{A}_2(\theta) = \mathbf{A}_1(\theta)\mathbf{E}$, where \mathbf{E} is a diagonal matrix with entries $[\mathbf{E}]_{m,m} = e^{-j\pi \sin(\theta_m)}$. Since $\mathbf{A}(\theta)$ spans the signal subspace, the relation between the signal subspaces of the sub-arrays, which we denote by \mathbf{U}_{S_1} and \mathbf{U}_{S_2} for $\mathbf{A}_1(\theta)$ and $\mathbf{A}_2(\theta)$, respectively, can be expressed as

$$\mathbf{U}_{S_2} = \mathbf{U}_{S_1} \mathbf{H}, \quad (11)$$

for some matrix \mathbf{H} . Since the eigenvalues of \mathbf{H} are equal to the diagonal elements of \mathbf{E} , by solving (11), i.e., extracting \mathbf{H} , one can recover the DoAs from these eigenvalues. Consequently, ESPRIT estimates the DoA vector as $\hat{\theta} = \sin^{-1}(\angle \text{eig}\{\mathbf{H}\}/\pi)$, where $\text{eig}\{\mathbf{H}\}$ is the vector representation of the eigenvalues of \mathbf{H} , and $\angle(\cdot)$ is the angle operator.

C. Problem Formulation

Subspace methods reliably estimate DoAs with an angular resolution that is not limited by the physical array, and they typically provide an interpretable visualization of the DoAs along with uncertainty measures. However, their reliance on Assumptions AS1-AS4 can be a limiting factor in various practical scenarios, which often involve broadband signals, coherent sources, miscalibrations, limited snapshots, and low SNR. Our goal is to design a method which enables subspace methods to operate also when AS1-AS4 do not hold.

In particular, we consider the recovery of θ from the observations matrix \mathbf{X} . While the number of sources M is not assumed to be a-priori known, we limit our attention to settings where M is smaller than the number of antenna elements N . Similarly, the number of snapshots T is not known during system design, though it is lower bounded by some T_{\min} (which can be as small as a single snapshot).

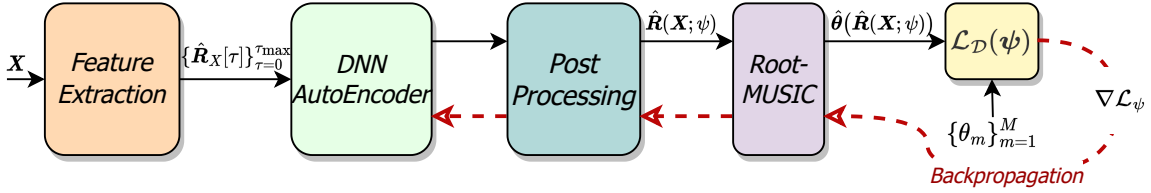
To alleviate reliance on AS1-AS4, we consider a data-aided setting, where one has access to a data set comprised of J pairs of observations and their corresponding DoAs, denoted

$$\mathcal{D} = \left\{ \left(\mathbf{X}^{(j)}, \theta^{(j)} \right) \right\}_{j=1}^J. \quad (12)$$

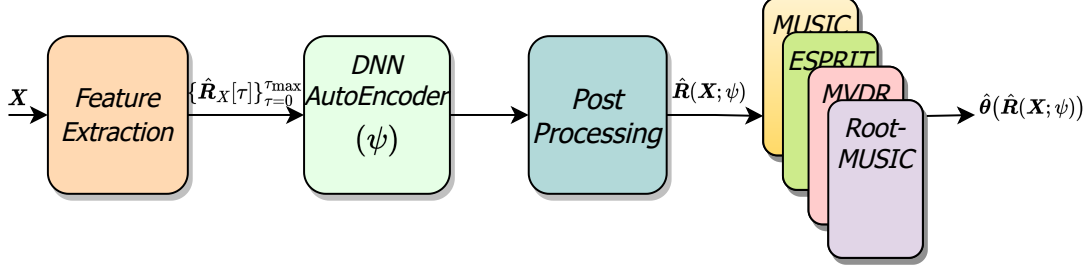
This data can be obtained from real-world sources or from synthetic data that closely resembles the signals that are expected to be detected. Different realizations can contain different numbers of sources M and different number of snapshots T , i.e., the dimensionality of $\theta^{(j)}$ and the number of columns of $\mathbf{X}^{(j)}$ can vary with the sample index j .

III. SUBSPACE NET

In this section we present the proposed SubspaceNet. We begin by discussing the high-level rationale of the algorithm and its architecture in Subsections III-A-III-B, respectively. Then, we present how SubspaceNet is trained and applied during inference in Subsections III-C-III-D, respectively, and provide a discussion in Subsection III-E.



(a) SubspaceNet training scheme



(b) SubspaceNet inference scheme

Fig. 2: High level illustration of SubspaceNet

A. High-Level Rationale

The reason that Assumptions **AS1-AS4** are critical for subspace methods follows from their role in the derivation of the orthogonality equality in (7). When these assumptions do not hold, one cannot reliably obtain an estimate of the input covariance that admits a decomposition into orthogonal signals and noise subspace associated with the . Based on the understanding that the sensitivity of subspace methods is encapsulated in the empirical covariance computation, we propose SubspaceNet. SubspaceNet augments subspace methods with deep learning as a form of model-based deep learning [23], [24], tackling the aforementioned challenges by providing a *surrogate* covariance matrix that can be divided into orthogonal signal and noise subspaces. To that aim, we employ a dedicated DNN that learns from data to produce the desired covariance. The architecture of the DNN is detailed in Subsection III-B. This surrogate covariance can then be used by different subspace methods, preserving their operation and interpretability, as discussed in Subsection III-D.

Since there is no 'ground truth' surrogate covariance, the DNN cannot be trained by comparing its output to a reference label, as commonly done in supervised learning. Instead, we evaluate the covariance produced by the DNN based on its usefulness for subspace-based DoA estimation. Consequently, the training loss is computed by comparing the DoAs available in (12) to the recovered DoAs at the output of the subspace DoA estimator employing the DNN, thus converting the DoA estimation algorithm into a discriminative model [25] that is trainable end-to-end. Since DNN training is based on first-order methods, the DoA estimator that processes the learned covariance during training has to be differentiable, i.e., one should be able to compute the gradient of the estimated DoAs with respect to the estimated covariance. Unlike MUSIC, whose mapping is based on non-differentiable peak-finding, Root-MUSIC is inherently differentiable, and is thus employed for training SubspaceNet, as discussed in Subsection III-C. The overall high-level design is presented in Fig. 2.

B. Architecture

The trainable architecture employed by SubspaceNet is designed to be able to map the input signal \mathbf{X} into an estimate of the covariance, denoted $\hat{\mathbf{R}}$, regardless of the number of snapshots T . This is done in three stages: extracting features from \mathbf{X} that are informative for the surrogate covariance estimation task; processing these features using a DNN-based autoencoder; and post-processing the DNN outputs to obtain an estimated covariance. We next elaborate on these stages.

1) *Feature Extraction*: Our design of the features used for computing the surrogate covariance draws inspiration from focusing techniques [27]. These approaches aim to convert broadband DoA recovery setups into surrogate narrowband ones by estimating the covariance as a linear combination of the input multivariate power spectral density. Since the power spectral density of a stationary signal is obtained as the Fourier transform of its auto-correlation function [28], we use the empirical auto-correlation of $\mathbf{x}(t)$ as our input features.

In particular, we fix a maximal number of lags $\tau_{\max} > 0$, which is not larger than the minimal number of snapshots T_{\min} . Then, for each $\tau \in \{0, \dots, \tau_{\max}\}$, we compute the empirical auto-correlation of \mathbf{X} as

$$\hat{\mathbf{R}}_X[\tau] = \frac{1}{T - \tau} \sum_{t=1}^{T-\tau} \mathbf{x}(t) \mathbf{x}^H(t + \tau). \quad (13)$$

The extracted features, processed by the DNN detailed next, are thus an $N \times N \times (\tau_{\max} + 1)$ tensor, i.e., its dimensionality does not depend on T . Consequently, this both provides the DNN with features that are considered to be informative for obtaining a useful surrogate covariance matrix, while allowing the DNN to be invariant of the number of snapshots T .

2) *DNN Autoencoder*: We utilize a DNN architecture inspired by denoising autoencoders to process $\{\hat{\mathbf{R}}_X[\tau]\}_{\tau=0}^{\tau_{\max}}$, as illustrated in Fig. 3. Autoencoders are a popular deep learning technique used for selecting relevant features from noisy data and mapping them into high-dimensional representations [29,

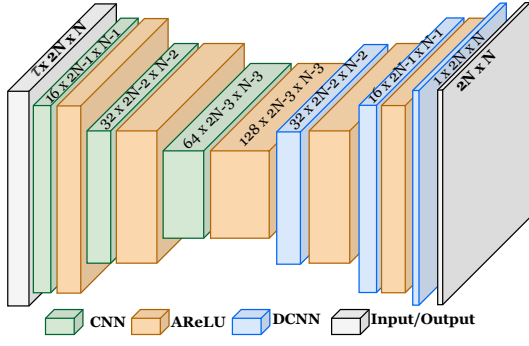


Fig. 3: SubspaceNet autoencoder architecture

Ch. 14]. The encoder part of the DNN consists of three CNN layers gradually increasing filter size. Its goal is to map the input into a lower dimensional latent representation that preserves only the meaningful information for the task, thus filtering out unnecessary information and noise. The decoder, which is comprised of a decreasing filter size deconvolutional neural network (DCNN) layers, aims to recover successive information details from the latent features as it progresses through its layers, producing a $2N \times N$ matrix which is post-processed into the surrogate covariance.

We use CNN layers with 2×2 kernels. This small kernel size allows to capture local phase correlations between neighboring sensors over the auto-correlation input, and potentially improve robustness to noise. The latter follows since the SNR across the spectrum is not constant, and thus the filters can detect local phase structures from the high SNR spectral regions to compensate for the lack of information from the low SNR regions. Unlike the conventional usage of CNN autoencoders in, e.g., computer vision, we do not employ pooling layers to avoid discarding useful spatial information. Instead of using common rectified linear unit activations $\text{ReLU}(x) = \max(0, x)$, we utilize anti-rectifier activations. This ensures that both positive and negative values are propagated, making it more suitable for sensory data containing both positive and negative values [30]. The anti-rectifier activation is expressed as the concatenation of both the positive and the negative part of the input, given by:

$$\text{ARReLU}(x) = [\text{ReLU}(x), \text{ReLU}(-x)]. \quad (14)$$

3) *Post-Processing*: The output of the autoencoder is a $2N \times N$ real matrix. To convert it into a surrogate covariance matrix, which is an $N \times N$ complex Hermitian positive definite matrix, we first reshape the output into a complex matrix $\mathbf{K} \in \mathbb{C}^{N \times N}$, by treating the first N rows as the real part and the remaining N rows as the imaginary part. To formulate the surrogate covariance, \mathbf{K} is converted into a Hermitian positive definite covariance estimate via

$$\hat{\mathbf{R}} = \mathbf{K}\mathbf{K}^H + \epsilon \mathbf{I}_N, \quad (15)$$

where $\epsilon > 0$ is a fixed hyperparameter of the architecture.

The trainable parameters of the architecture are the weights of the autoencoder, denoted ψ . We thus write the overall mapping as $\hat{\mathbf{R}}(\mathbf{X}; \psi)$, encompassing the feature extraction, DNN processing, and output reshaping stages.

C. Training

The training procedure uses the dataset \mathcal{D} (12) to tune the parameters ψ such that the surrogate covariance $\hat{\mathbf{R}}(\mathbf{X}; \psi)$ is useful for subspace-based DoA recovery, i.e., it can be decomposed into orthogonal subspaces encapsulating the signals and the noise. This is achieved by encouraging $\hat{\mathbf{R}}(\mathbf{X}; \psi)$ to be a covariance matrix using which the DoAs recovered by Root-MUSIC, denoted $\hat{\boldsymbol{\theta}}(\hat{\mathbf{R}}(\mathbf{X}; \psi))$, is an accurate estimate of $\boldsymbol{\theta}$. To describe how this is carried out, we first discuss the loss measure, after which we explain the training procedure.

1) *Loss Measure*: The loss function evaluates the quality of DoA estimation by comparing the DoAs recovered by Root-MUSIC combined with SubspaceNet. While in principle one can utilize standard loss measures for regression tasks, e.g., mean-squared error, when evaluating DoA recovery, one has to account for the following properties:

- P1 DoAs are periodic quantities, i.e., estimating $\hat{\boldsymbol{\theta}} + 2\pi$ is the same as $\hat{\boldsymbol{\theta}}$. Thus the difference between an angle and its estimate does not necessarily correspond to actual error.
- P2 DoA estimation is invariant to the order of the predicted DoAs, e.g., estimating $\hat{\boldsymbol{\theta}} = [\theta_1, \theta_2]^T$ is equivalent to outputting $\hat{\boldsymbol{\theta}} = [\theta_2, \theta_1]^T$.
- P3 The number of signals \hat{M} is also estimated, and may thus differ from the true M , i.e., the cardinality of the output may not be equal to that of the ground-truth DoAs.

To account for P1, we employ the root mean squared periodic error (RMSPE) loss [31], which evaluates the element-wise error over the periodic range. We extend this measure to be permutation invariant by P2, by modifying the RMSPE loss to compare all possible combinations of predicted DoAs with the ground truth labels. To cope with P3, we treat cases where $\hat{M} < M$ by setting the last $M - \hat{M}$ DoAs recovered on $\hat{\boldsymbol{\theta}}$ to be zero when evaluating the loss.

The resulting loss function is used to evaluate SubspaceNet when applied with Root-MUSIC to input \mathbf{X} originating from DoAs $\boldsymbol{\theta}$ while accounting for P1-P3. It is given by

$$l(\mathbf{X}, \boldsymbol{\theta}; \psi) = \min_{\mathbf{P} \in \mathcal{P}} \left(\frac{1}{M} \left\| \text{mod}_{\pi} \left(\boldsymbol{\theta} - \mathbf{P}\hat{\boldsymbol{\theta}}(\hat{\mathbf{R}}(\mathbf{X}; \psi)) \right) \right\|^2 \right)^{\frac{1}{2}},$$

where mod_{π} denotes the modulo operation with respect to the angle range of interest, i.e., $[-\pi/2, \pi/2]$, and \mathcal{P} is the set of set of all $M \times M$ permutation matrices, i.e., binary matrices where each row and column contains a single non-zero entry. The loss evaluated over a dataset \mathcal{D} is computed as

$$\mathcal{L}_{\mathcal{D}}(\psi) = \frac{1}{|\mathcal{D}|} \sum_{(\mathbf{X}^{(j)}, \boldsymbol{\theta}^{(j)}) \in \mathcal{D}} l(\mathbf{X}^{(j)}, \boldsymbol{\theta}^{(j)}; \psi), \quad (16)$$

2) *Training Procedure*: The selection of Root-MUSIC as our model-based estimator for training SubspaceNet, is attributed to the differentiability of its mapping. Specifically, the DoA estimates are obtained from the roots of the polynomial equation (10), which can be expressed as an implicit polynomial function. Implicit differentiation makes it possible to compute the derivative of the polynomial roots, that are used for the estimated DoAs in Root-MUSIC, with respect to its coefficients $\{f_n\}$ [32]. These coefficients $\{f_n\}$ are obtained

from the EVD of the estimated covariance matrix, and are thus differentiable with respect to it, see, e.g., [33].

The above property allows end-to-end optimization of the DNN parameters of SubspaceNet using first-order methods, e.g., stochastic gradient descent (SGD) and its variants. In particular, automatic differentiation engines, e.g., Autograd [34], can compute the gradient of the loss (16) with respect to the trainable parameters ψ by backpropagating through the Root-MUSIC block in Fig. 2a. The training procedure of SubspaceNet using SGD is detailed as Algorithm 1.

Algorithm 1: SubspaceNet Training using SGD

Init: Lags τ_{\max} , hyperparameter ϵ , learning rate μ , number of batches B , epochs number e_{\max} .
Input: Training set \mathcal{D}

- 1 Initialize CNN weights ψ ;
- 2 **for** epoch = 0, 1, ..., e_{\max} **do**
- 3 Randomly divide \mathcal{D} into B batches $\{\mathcal{D}_b\}_{b=1}^B$;
- 4 **for** $b = 1, 2, \dots, B$ **do**
- 5 **for** $(\mathbf{X}_b^{(j)}, \theta_b^{(j)}) \in \mathcal{D}_b$ **do**
- 6 Compute $\hat{\mathbf{R}}(\mathbf{X}_b^{(j)}; \psi)$ with SubspaceNet;
- 7 Use Root-MUSIC to get $\hat{\theta}(\hat{\mathbf{R}}(\mathbf{X}_b^{(j)}; \psi))$;
- 8 Compute $\mathcal{L}_{\mathcal{D}_b}(\psi)$ using (16);
- 9 Update weights via $\psi \leftarrow \psi - \mu \nabla_{\psi} \mathcal{L}_{\mathcal{D}_b}(\psi)$;
- 10 **return** ψ

D. Inference

We employ Root-MUSIC during training due to its differentiability. However, once trained, SubspaceNet can be seamlessly incorporated into any classical subspace methods such as MUSIC and ESPRIT, producing a covariance matrix which facilitates DoA estimation, as presented in Fig. 2b. The inference algorithm is summarized in Algorithm 2. This plug-and-play feature is a significant advantage, as it can notably enhance the performance of classical methods and enable them to operate reliably in harsh settings where AS1-AS4 do not hold, i.e., where the original MB algorithms typically fail. This is thanks to the fact that the learned surrogate covariance matrix enables the algorithms to operate as if AS1-AS4 are satisfied, thus they can precisely distinguish between the noise and signal subspaces, as we demonstrate in Section IV.

While the presentation of SubspaceNet so far considers subspace-based DoA estimation, the fact that it learns a covariance that facilitates DoA recovery can also be utilized by other forms of covariance-based methods. For instance, in our numerical study in Section IV we show that the covariance computed by SubspaceNet can be utilized by minimum variance distortionless response (MVDR) [35], which processes the covariance representation without requiring its decomposition into signal and noise subspace. We demonstrate that combining MVDR with SubspaceNet enables coping with settings where the beamformer typically struggles, e.g., coherent sources.

E. Discussion

The proposed SubspaceNet leverages data by using deep learning tools to enable subspace methods to operate reliably

Algorithm 2: SubspaceNet Inference

Init: Trained SubspaceNet parameters ψ , model-based subspace DoA estimator
Input: Observations \mathbf{X} ;

- 1 Apply to SubspaceNet \mathbf{X} to obtain $\hat{\mathbf{R}}(\mathbf{X}; \psi)$;
- 2 Apply subspace method to estimate $\hat{\theta}$ from $\hat{\mathbf{R}}(\mathbf{X}; \psi)$;
- 3 **return** $\hat{\theta}$

in the presence of coherent sources, broadband signals, limited snapshots, miscalibrated arrays, and low SNR. This is achieved by identifying that the difficulty in dealing with these challenges is associated with the computation of the covariance matrix. Thus, we propose a dedicated DNN architecture which learns to provide a surrogate covariance, by training its output to be useful for Root-MUSIC-based DoA recovery.

As opposed to [21], which focused on MUSIC and had to modify its operation for training, the inherent differentiability of Root-MUSIC allows to train the architecture end-to-end without affecting how the computed covariance is processed. This allows the trained architecture to not only achieve accurate DoA estimation in harsh conditions, but also to allow the subspace methods applied to produce a meaningful spectrum, as demonstrated in Section IV.

The derivation of SubspaceNet considers DoA recovery with ULAs, as detailed in Subsection II-A. However, its formulation can be extended to other forms of arrays where subspace methods are applied for DoA recovery, including planar arrays [36], circular arrays [37], and sparse arrays [38]. For the latter, the ability of SubspaceNet to learn to overcome array mismatches, as presented in Section IV, makes it extremely attractive. We leave these extensions of SubspaceNet for future study.

IV. NUMERICAL EVALUATION

In this section, we empirically evaluate SubspaceNet when applied with different subspace and covariance-based estimation algorithms¹. Our experiments cover scenarios where assumptions AS1-AS4 are not necessarily satisfied, and demonstrate the ability of SubspaceNet to enable classic DoA estimators to operate in these settings while preserving performance and interpretability. We first detail the experimental setup in Subsection IV-A, after which we report the performances achieved under these setups in Subsection IV-B. We conclude by investigating the interpretability of SubspaceNet when combined with different model-based methods in Subsection IV-C.

A. Experimental Setup

1) *Signal Model:* Throughout this study, we consider a ULA consisting of $N = 8$ sensors with M impinging signals, where we simulate different values of M . Except for the study reported in Subsection IV-B3, where we consider broadband settings, the signals are generated according to (1), i.e., representing a narrowband case. The DoAs are uniformly generated from the interval $[-\frac{\pi}{2}, \frac{\pi}{2}]$. The SNR is defined as the inverse of the noise variance, i.e., $\text{SNR} = 1/\sigma_v^2$.

¹The source code used in our empirical study along with the hyperparameters is available at <https://github.com/ShlezingerLab/SubspaceNet>

2) *SubspaceNet Architecture*: As detailed in Subsection III-B, SubspaceNet is comprised of a DNN autoencoder with non-trainable preceding and subsequent processing. The auto-correlation features in (13) are extracted for maximal lag of $\tau = \min(8, T - 1)$. The autoencoder architecture utilized is composed of three convolution layers, having 16, 32, and 64 output channels, respectively. These are followed by three deconvolution layers with 32, 16, and 1 output channels, respectively. The kernel size of each layer is set to 2×2 . The output of the autoencoder is reshaped into a surrogate covariance via (15) with $\epsilon = 1$. The overall number of trainable parameters is 41,761. The architecture is trained using the Adam optimizer [39] with learning rate $\mu = 0.001$. For brevity, we use the abbreviated term *SubNet* for SubspaceNet in the figure legends in the sequel.

3) *DoA Estimators*: To assess the ability of SubspaceNet to improve classic subspace methods, we evaluate the classic subspace methods detailed in Subsection II-B, i.e., MUSIC, Root-MUSIC, and ESPRIT, comparing their performance when combined with SubspaceNet to that achieved when applied with the standard empirical covariance. Specifically, when employing MUSIC, we detect the DoAs from the spectrum by searching for the peaks over a grid with resolution 0.5° (0.0087 [rad]).

In settings where AS1-AS4 do not hold, we contrast SubspaceNet with representative model-based extensions of classic subspace methods designed to cope with each scenario. In particular, for coherent sources, we employ SPS pre-processing, which is a widely adopted model-based approach for coping with such scenarios [6], [7]. To evaluate DoA estimation under broadband settings, we compare SubspaceNet with model-based extensions for broadband signals based on the technique proposed in [27]. This involves dividing the relevant frequency spectrum into bins, and then applying classical narrowband subspace methods to each bin separately, while aggregating the results to yield a broadband estimate.

We also compare SubspaceNet to alternative DNN-based DoA estimators. We consider two data-driven benchmarks: 1) a CNN-based DoA estimator based on the architecture proposed in [12] coined *CNN*, representing a black-box DNN design; 2) *DA-MUSIC* of [21], which interconnects a recurrent neural network and a fully-connected architecture following the flow of MUSIC. All data-driven DoA estimators are trained on the same data, comprised of $J = 45000$ samples corresponding to SNR of 10 dB (unless stated otherwise). For the *CNN* model, a grid of classes with a resolution of 0.5° is defined (as used in MUSIC), resulting in over $21 \cdot 10^6$ trainable parameters, while *DA-MUSIC* has 10,194 trainable parameters. Following the approach used in [12], a dataset containing $\binom{M}{361}$ combinations of angles is generated for each tested SNR, resulting in an extensive set of over 300,000 samples for training the *CNN* model.

B. DoA Recovery Performance

Here, we evaluate the accuracy of SubspaceNet, measured via the RMSPE. We consider settings with coherent sources (not holding AS2); with dominant noise and limited snapshots (not holding AS4); with broadband signals (not holding AS1);

RMSPE [rad]	$M = 2$	$M = 3$	$M = 4$
<i>Root-MUSIC</i>	0.2178	0.356	0.405
<i>SPS-Root-MUSIC</i>	0.01765	0.02857	0.212
<i>SubspaceNet+Root-MUSIC</i>	0.0035	0.0126	0.0678
<i>MUSIC</i>	0.1653	0.333	0.398
<i>SPS-MUSIC</i>	0.0451	0.04074	0.31996
<i>SubspaceNet+MUSIC</i>	0.0368	0.074	0.0916
<i>ESPRIT</i>	0.45104	0.392	0.405
<i>SPS-ESPRIT</i>	0.0161	0.0649	0.219
<i>SubspaceNet+ESPRIT</i>	0.00831	0.0425	0.078
<i>DA-MUSIC</i>	0.0207	0.0464	0.0693
<i>CNN</i>	0.013427	0.02171	0.1295

TABLE I: DoA accuracy, coherent sources.

and with miscalibrated arrays (not holding AS3). We empirically evaluate the RMSPE by averaging over 5000 Monte Carlo trials. To focus on the ability to identify the DoAs correctly, here we set \hat{M} to the true number of DoAs M , while in Subsection IV-C we show that \hat{M} can indeed be extracted as an accurate estimate of M . For ease of presentation, figures comparing DoA estimators versus SNR report performance in terms of mean squared periodic error in dB.

1) *Coherent Sources*: We first evaluate the ability of SubspaceNet to effectively handle coherent sources. We focus on the challenging fully coherent case, where all sources exhibit identical phases and amplitudes, resulting in \mathbf{R}_S having minimal unit rank. We simulate different numbers of narrowband coherent sources estimated from $T = 100$ snapshots, with an SNR of 10 dB and a calibrated ULA.

The RMSPE results achieved by the considered DoA estimators are reported in Table I. We observe in Table I that SubspaceNet augmentation enables effective and consistent handling of coherent sources, improving the performance of all considered model-based algorithms. Notably, the augmentation of Root-MUSIC with SubspaceNet on $M = 2$ sources leads to almost $60\times$ better estimation performance than classical Root-MUSIC. Even when a dedicated SPS technique is used to increase the empirical covariance rank, the SPS Root-MUSIC algorithm results are inferior to SubspaceNet. We also observe that while SubspaceNet was trained with Root-MUSIC, its surrogate covariance also notably facilitates the operation of MUSIC and ESPRIT, which both exhibit improvement in estimation performance compared to classical and pre-processed estimation methods. Moreover, SubspaceNet outperforms the data-driven benchmarks, while using much less parameters than *CNN* model and maintaining a similar scale of parameter quantity as *DA-MUSIC*, without limiting the interpretability of model-based DoA estimators, as shown in Subsection IV-C.

2) *Low SNR and Few Snapshots*: We proceed to evaluate the ability of SubspaceNet to facilitate coping with low SNRs and a limited number of snapshots. Such conditions are recognized to profoundly deteriorate model-based DoA estimation. To pinpoint the gains of SubspaceNet, we first consider only low SNRs with $M = 2$ non-coherent sources, after which we limit the number of snapshots, and then replace the sources with coherent ones, while systematically contrasting SubspaceNet-aided DoA estimators with the classic model-based operation for each scenario. In experiments conducted

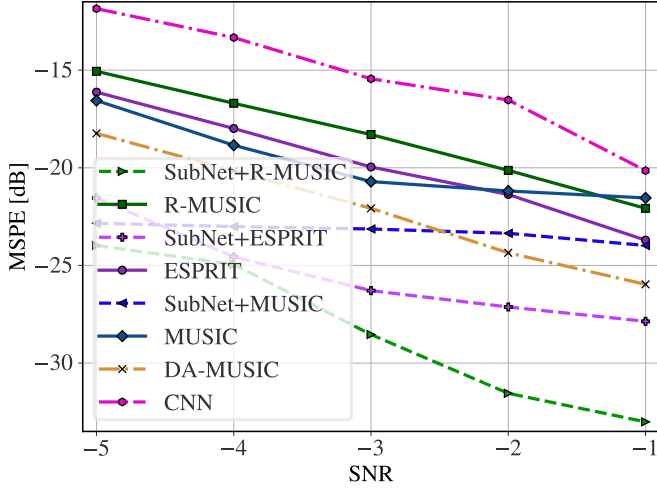


Fig. 4: DoA estimation MSPE, $T = 200$, non-coherent sources

with multiple SNRs, the training data used by data-driven estimators is that of the lowest SNR considered in the range.

We thus commence with considering highly noisy observations with SNRs in the range of $[-5, 0]$ dB. The signals are non-coherent and the number of snapshots is $T = 200$. The results, reported in Fig. 4, demonstrate that SubspaceNet augmentations notably improve the ability of subspace-based DoA estimators in coping with high noise levels. These results emphasize that SubspaceNet can not only mitigate the harmful effects of coherency, but also effectively enhance the SNR, leading to improved accuracy in DoA estimation.

We proceed to considering the challenging setting where merely $T = 2$ snapshots are employed. Here, we set the SNR to be in the range of $[5, 10]$ dB. The resulting DoA estimation accuracy, depicted in Fig. 5, clearly shows that the incorporation of SubspaceNet into classical model-based methods enables them to effectively handle few observations, even in a scenarios where these methods are typically unfeasible, i.e., where the number of snapshots is not larger than the number of sources. Moreover, the performance of SubspaceNet continues to improve as the SNR increases, while the estimation accuracy of classical model-based methods is dominated by their inability to cope with few snapshots, and thus does not notably improve with SNR.

We next introduce coherent sources, assessing the ability of SubspaceNet in handling settings not meeting both AS2 and AS4. We compare the augmentation of subspace methods with SubspaceNet to their model-based counterparts in Fig. 6 under low SNRs with $T = 200$ snapshots (Fig. 6a) and under moderate SNRs with merely $T = 20$ and $T = 2$ snapshots (Figs. 6b-6c, respectively). The results show that the surrogate covariance of SubspaceNet enables reliable subspace-based DoA estimation even in an extreme scenario where AS2 and AS4 are both violated. This is also evident in Table II, which reports the RMSPE values achieved for SNR of 5 dB, comparing SubspaceNet also to the data-driven benchmarks, whose performance is inferior to that of SubspaceNet.

3) *Broadband settings*: The scenarios considered so far were all based on the narrowband formulation in (1). Here, we evaluate SubspaceNet under broadband settings. In such

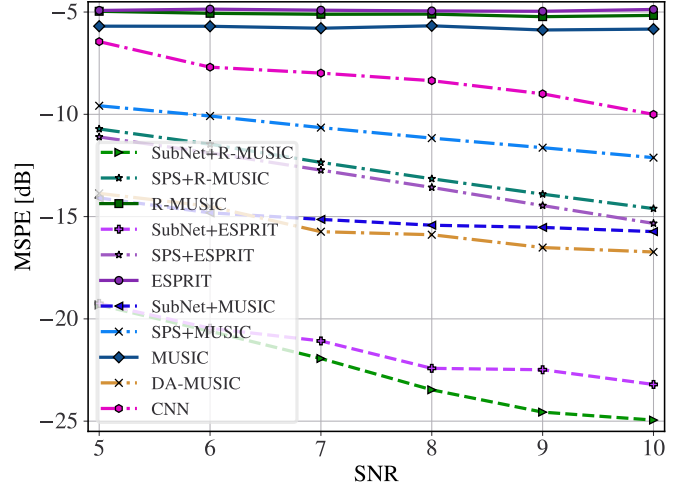


Fig. 5: DoA estimation MSPE, $T = 2$, non-coherent sources

Algorithm	RMSPE [rad]
<i>MUSIC</i>	0.45053
<i>SPS+MUSIC</i>	0.14095
<i>SubspaceNet+MUSIC</i>	0.039327
<i>ESPRIT</i>	0.50725
<i>SPS+ESPRIT</i>	0.1923
<i>SubspaceNet+ESPRIT</i>	0.03434
<i>Root-MUSIC</i>	0.4600
<i>SPS+Root-MUSIC</i>	0.1444
<i>SubspaceNet+Root-MUSIC</i>	0.0330
<i>DA-MUSIC</i>	0.0826
<i>CNN</i>	0.167645

TABLE II: $M = 2$ coherent signals, $T = 2$, SNR=5 dB

cases, one can formulate the signal model in the frequency domain, which at frequency ω is given by [27]

$$\mathcal{X}(\omega) = \mathbf{A}(\omega, \boldsymbol{\theta})\mathcal{S}(\omega) + \mathcal{V}(\omega). \quad (17)$$

In (1), $\mathcal{X}(\omega)$ and $\mathcal{S}(\omega)$ are the discrete-time multivariate Fourier transforms of $\mathbf{x}(t)$ and $\mathbf{s}(t)$, respectively, $\mathcal{V}(\omega)$ is noise, and the steering vectors comprising $\mathbf{A}(\omega, \boldsymbol{\theta})$ are

$$\mathbf{a}(\omega, \theta) = \left[1, e^{-j\omega \frac{d}{c} \sin \theta}, \dots, e^{-j\omega(M-1) \frac{d}{c} \sin \theta} \right], \quad (18)$$

with d denoting the element spacing of the ULA, and c being the propagation velocity.

We simulate the time-domain broadband signals using orthogonal frequency-division multiplexing (OFDM) with L sub-carriers, where each carrier, denoted $s_{m,l}$ for the l th subcarrier of the m th signal, is modulated independently with a zero-mean complex-Gaussian unit variance distribution. The overall OFDM signal can be expressed as:

$$\mathbf{s}_m^{(\text{OFDM})}(t) = \frac{1}{L} \sum_{l=0}^{L-1} s_{m,l} e^{2\pi j l \frac{B_f}{L f_s} t} \quad (19)$$

where f_s is the sampling frequency, and B_f is the signal bandwidth. The acquired observations are generated following (17), where the inter-element spacing is given by half the minimal wavelength $d = c/2B_f$. We generate $M = 2$ OFDM

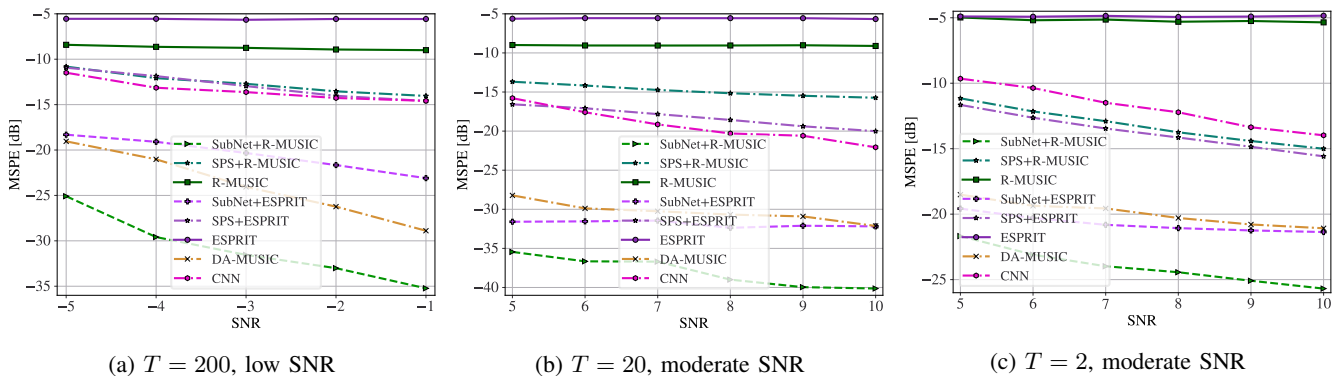


Fig. 6: DoA estimation, SNR & minor snapshots, coherent sources

Algorithm	RMSPE [rad]
<i>MUSIC</i>	0.4669
<i>Broadband MUSIC</i>	0.1233
<i>DA MUSIC</i>	0.08282
<i>CNN</i>	0.46677
<i>SubspaceNet+MUSIC</i>	0.0399
<i>SubspaceNet+ESPRIT</i>	0.0648
<i>SubspaceNet+Root-MUSIC</i>	0.0408

TABLE III: RMSPE results, $M = 2$ broadband OFDM signals

signals with $L = 500$ subcarriers, setting $B_f = 0.5$ kHz. Various sampling rates ranging from 50 to 1000 Hz are tested, while the signals are observed for a duration of 1 second, thus the number of snapshots is $T = 1/f_s$. The performance of SubspaceNet is evaluated for all sampling rates, despite being trained solely on observations sampled at 0.2 kHz.

We evaluate the performance of MUSIC, Root-MUSIC, and ESPRIT when combined with SubspaceNet and when using the conventional empirical covariance, as well as compared to the broadband extension of MUSIC proposed in [27] which divides the bandwidth into 50 separate bins. The results, depicted in Fig. 7, consider both non-coherent as well as coherent sources. The non-coherent results depicted in Fig. 7a demonstrate that the incorporation of SubspaceNet models leads to significantly improved performance in comparison to narrowband methods and the broadband extension of MUSIC. SubspaceNet consistently enables reliable DoA estimation, even when a minimal number of snapshots are available, with $f_s = 50$ Hz. These findings also hold when the sources are coherent, as demonstrated in Fig. 7b. In contrast, as expected, the subspace model-based broadband extension is unable to estimate DoAs under both coherent and broadband conditions.

To numerically capture the exact gains of SubspaceNet, we report the RMSPE values achieved by SubspaceNet in the broadband setting with $M = 2$ coherent sources and a sampling rate of $f_s = 200$ Hz in Table III. We also include the accuracy achieved by the data-driven DA-MUSIC and CNN benchmarks. Table III showcases that SubspaceNet allows model-based subspace methods to achieve substantially improved accuracy in broadband settings, surpassing the data-driven benchmarks, as well as model-based methods designed for broadband settings, whose inference procedure is more complex as they require separate DoA estimation for each bin.

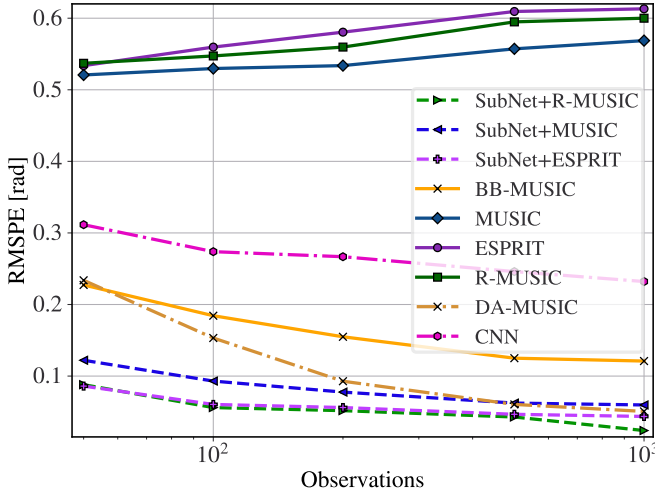
4) *Array Miscalibration*: Here, we investigate the effectiveness of SubspaceNet in learning from data to handle array miscalibrations. The calibration of the array manifold is a critical aspect of DoA estimation, as inaccurate calibration can lead to substantial errors. We simulate two forms of miscalibrations, which both cause the actual array response to deviate from the ideal pattern, significantly affecting the performance of subspace methods. In both scenarios, the received signal is comprised of $M = 2$ non-coherent signals.

In the first scenario, array distance miscalibration is simulated, where the spacing between each pair of sensors deviates from the standard ULA configuration of half-wavelength, resulting in non-uniform element spacing. The spacing between each adjacent pair of sensors in the m th position is established as the nominal half-wavelength distance d plus a uniformly distributed random variable denoted as $\delta_m \sim U(-\eta, \eta)$, where η is the percentage of deviation from the nominal spacing. Consequently, the steering vector in (2) becomes miscalibrated, with its m th element now given by

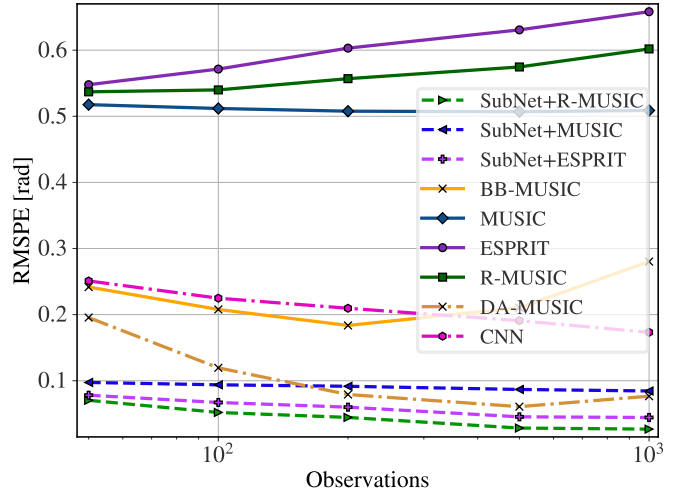
$$[\mathbf{a}(\theta)]_m \triangleq e^{-2\pi j \frac{(d+\delta_m)(m-1)}{c} \sin(\theta)}, \quad m \in \{1, \dots, M\}. \quad (20)$$

The resulting RMSPE values achieved by subspace-based DoA estimators with and without SubspaceNet are reported in Fig. 20, for different values $\eta \in [0.0125d, 0.075d]$, i.e., a maximum deviation of 30% from the calibrated spacing. The results depicted in Fig. 8a underscore the ability of SubspaceNet to deal with discrepancies in the array geometry, particularly when the steering vector is affected by non-uniform (and non-nominal) elements spacing. In contrast, classical subspace methods heavily rely on the nominal ULA form of the array manifold, yielding non-optimal estimation as η increases.

In the second scenario, we introduce miscalibration directly in the steering vector, rather than in the element spacing. This is achieved by adding a zero-mean complex-Gaussian noise with variance σ_{sv}^2 to each element in the steering vector, resulting in mismatches in the creation of the subspace core equation (7). The simulation results depicted in Fig. 8b further indicate that SubspaceNet indeed exhibits superior performance over traditional subspace methods when handling steering vector corruption due to the addition of zero-mean Gaussian noise, resulting in more accurate DoA estimation. On the other hand, classical subspace methods appear to be highly sensitive to this



(a) Non-coherent OFDM signals



(b) Coherent OFDM signals

Fig. 7: Broadband DoA estimation comparison, for various observations

type of corruption, leading to poor estimation results as the noise variance increases. Additionally, the results indicate that the performance gap between traditional subspace methods and SubspaceNet increases as the level of steering vector corruption increases, for both $\sigma_{sv}^2 = 0.75$ and $\eta = 0.075d$. This suggests that SubspaceNet could potentially provide more significant benefits in scenarios with higher levels of noise corruption and geometry mismatches, making it a promising solution for applications in challenging environments.

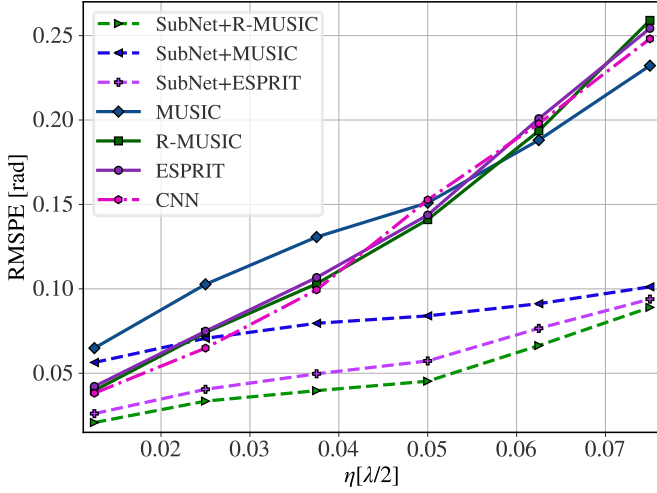
C. Interpretability

The results presented so far systematically demonstrate that the augmentation of subspace methods with SubspaceNet enables these classic algorithms to operate reliably in scenarios where their traditionally limiting assumptions **AS1-AS4** do not hold. Specifically, SubspaceNet outputs a surrogate covariance matrix which enables subspace methods to operate in an unaltered manner in various challenging scenarios: It can efficiently cope with wideband signals; accurately resolve coherent signals; operate reliably with few snapshots and high noise levels; and boost robustness to different forms of miscalibrations. These gains stem from the fact that SubspaceNet leverages the abstractness of DNNs to learn a desirable mapping from data, which here is the extraction of a suitable covariance matrix. An additional key gain of SubspaceNet, which is not shared by conventional DNN-based solutions, is its ability to preserve the desirable interpretable operation of model-based DoA estimators, and in fact provide meaningful visual representations associated with classic methods in settings where these are typically not achievable. To show this property of SubspaceNet, we first visualize its ability to yield distinguishable signal and noise subspaces. Then we show the spectrum representations obtained by MUSIC and Root-MUSIC when combined with SubspaceNet, after which we demonstrate that SubspaceNet can yield meaningful beampatterns when combined with covariance-based beamformers that are not necessarily based on subspace methods, such as MVDR.

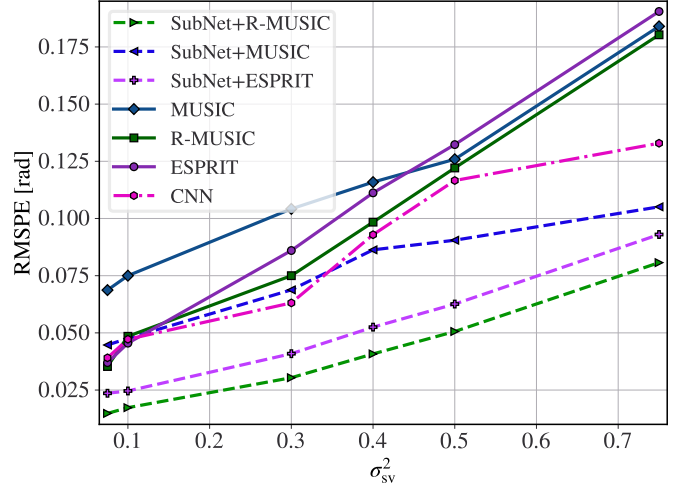
1) *Subspace Separation*: We commence with a comparison of the normalized covariance eigenvalues produced by SubspaceNet compared with the conventional and the SPS-aided empirical estimation of the covariance for coherent sources. The results, depicted in Fig. 9, demonstrate that SubspaceNet yields a clear separation between the $M = 3$ dominant eigenvalues of the signal subspace and those associated with noise. In contrast, conventional empirical estimation is only capable of identifying one eigenvalue associated with the signal subspace, whereas the SPS empirical estimation method can identify only two eigenvalues, with the remaining eigenvalues attributed to the noise subspace. The capability of SubspaceNet to distinguish between the two subspaces significantly enhances resolving coherent sources compared to model-based subspace methods.

2) *Spectrum Presentation*: When assumptions **AS1** to **AS4** hold, subspace methods demonstrate informative spectral representations that are strongly correlated with the true DoAs. Specifically, the MUSIC spectrum displays distinct peaks at the DoA angles, while the Root-MUSIC polar spectra exhibit roots and eigenvalues corresponding to the DoA locations on the unit circle. We next investigate the spectral behavior of each subspace method and its SubspaceNet augmentation, over the following scenarios in which **AS1-AS4** are violated:

- 1) DoA estimation of narrowband coherent sources, i.e., **AS2** does not hold. The DoAs are located at $\theta = [-12.34^\circ, 34.56^\circ, 65.78^\circ]$, and are observed via $T = 100$ snapshots at SNR of 10 dB. The resulting MUSIC and Root-MUSIC spectra are illustrated in Fig. 10.
- 2) Scenario where **AS2** and **AS4** do not hold, using the same settings as in the study reported in Table II, with sources at $\theta = [23.45^\circ, 56.78^\circ]$. The resulting MUSIC and Root-MUSIC spectra are illustrated in Fig. 11.
- 3) DoA estimation of broadband coherent sources, located at $\theta = [-45.67^\circ, -23.45^\circ]$, from $T = 50$ snapshots. The model-based spectrum here is no longer informative in representing the true DoA, as illustrated in Fig. 12.



(a) Mismatch due to deviation from half-wavelength spacing



(b) Mismatch due to noisy steering vectors

Fig. 8: Miscalibrated array DoA estimation comparison

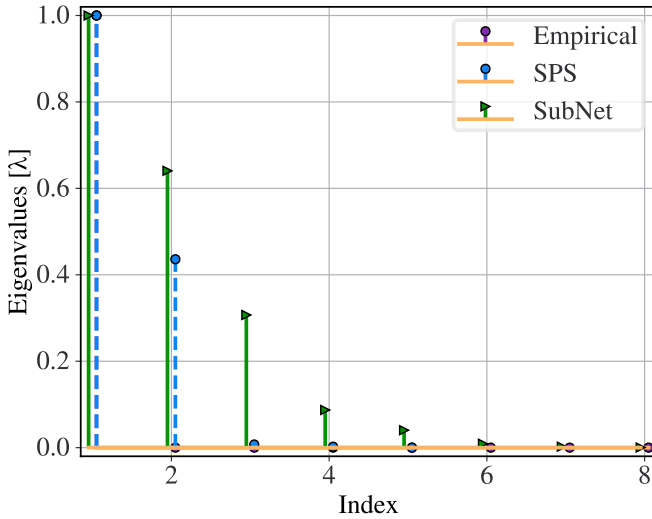


Fig. 9: Normalized eigenvalues of empirical, SPS and SubspaceNet covariance matrices. $M = 3$ coherent sources.

We observe in Figs. 10-12, that SubspaceNet produces an interpretable and informative spectrum. The roots closest to the unit circle in the SubspaceNet+Root-MUSIC spectrum (Figs. 10c-12c) and the distinct peaks in the SubspaceNet+MUSIC spectrum (Figs. 10a-12a) can be easily linked to the actual DoAs. On the other hand, classical MUSIC and Root-MUSIC algorithms are unable to produce meaningful spectrum representations. While MUSIC spectrum for narrowband coherent sources (Fig. 10a) may reveal minor peaks near the source angles, it horribly fails to provide any meaningful information for the scenarios depicted Figs. 11a-12a. Furthermore, SubspaceNet enables a more distinguishable spectrum. As shown in Figs. 10c-12c, the non-DoA roots are pushed further away from the unit circle, facilitating their distinction from true DoA roots. The resulting Root-MUSIC spectrum becomes more interpretable, especially in challenging scenarios. This is clearly observed in the scenario with a

small number of snapshots in Fig. 11c, where a non-DoA root which located close to the true DoA, at $\theta = 28.4^\circ$, is pushed from the unit circle ($|\text{root}| > 8$), preventing misclassification.

3) *Beamforming Pattern*: We conclude by demonstrating that the surrogate covariance produced by SubspaceNet is useful not only for subspace methods, but also for other forms of covariance-based array processing algorithms. To exemplify this, we consider MVDR [35], which is a popular beamforming method that enhances the signal power in the desired direction while suppressing noise and interference. This results in a beam pattern that provides valuable information about the directions of the sources of interest. Although MVDR does not rely on subspace decomposition for its beamforming operation, it employs the covariance matrix to shape its pattern, and hence it is subject to the same empirical estimation limitations as classical subspace methods, and its effectiveness is still limited by the accuracy of the covariance matrix estimate.

To show that SubspaceNet facilitates the operation of MVDR, we visualize the beam pattern achieved by MVDR with and without SubspaceNet augmentation in Fig. 13, under the same settings used in Subsection IV-C2. The beam patterns depicted in Fig. 13 clearly demonstrate the superiority of SubspaceNet in producing surrogate covariance matrices that are useful not only for DoA estimation subspace methods, but also to obtain high resolution effective beam patterns. Specifically, Figs. 13a-13b demonstrate that SubspaceNet produces narrow lobes in the direction of the sources, enhancing the discrimination between sources, and mitigating interference by reducing the power in non-DoA directions. When using the conventional empirical covariance, MVDR exhibits limitations in achieving these objectives in scenarios with multiple coherent sources and low SNR. Additionally, like subspace methods, MVDR is inherently limited in its ability to handle broadband sources. This shortcoming leads to a beam pattern that deviates significantly from the true DoAs, as shown in Fig. 13a. Nonetheless, by integrating the SubspaceNet augmentation, the received signal power in the desired directions is amplified,

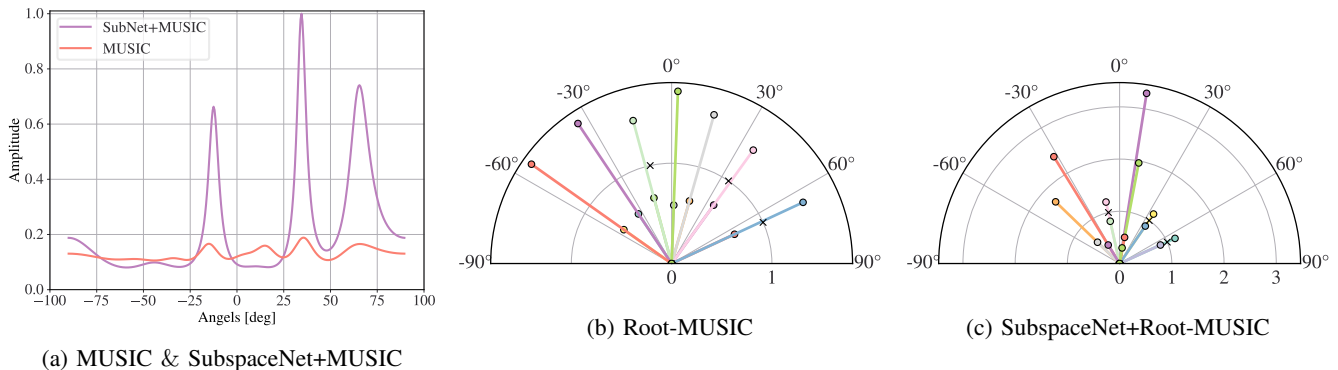


Fig. 10: Spectrum representation: $M = 3$ narrowband coherent sources

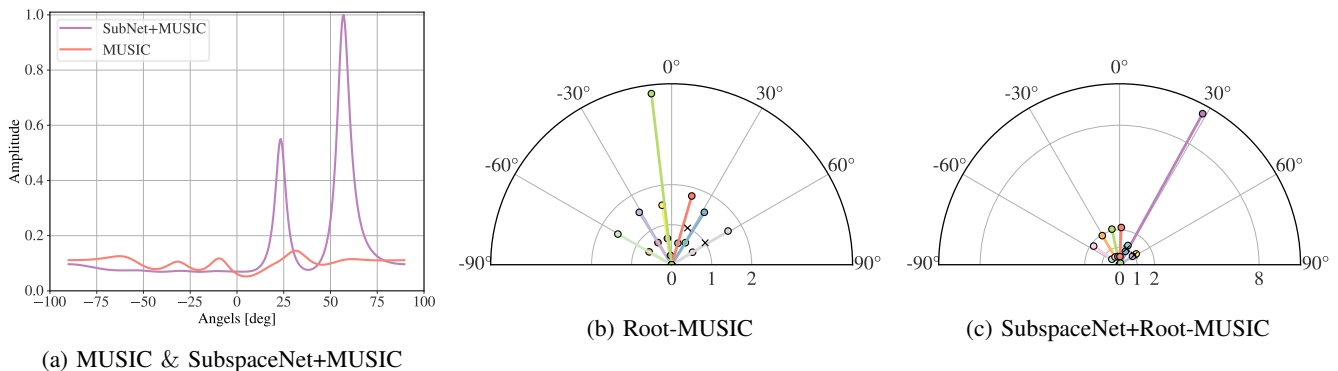


Fig. 11: Spectrum representation: $M = 2$ narrowband coherent sources with few snapshots & moderate SNR

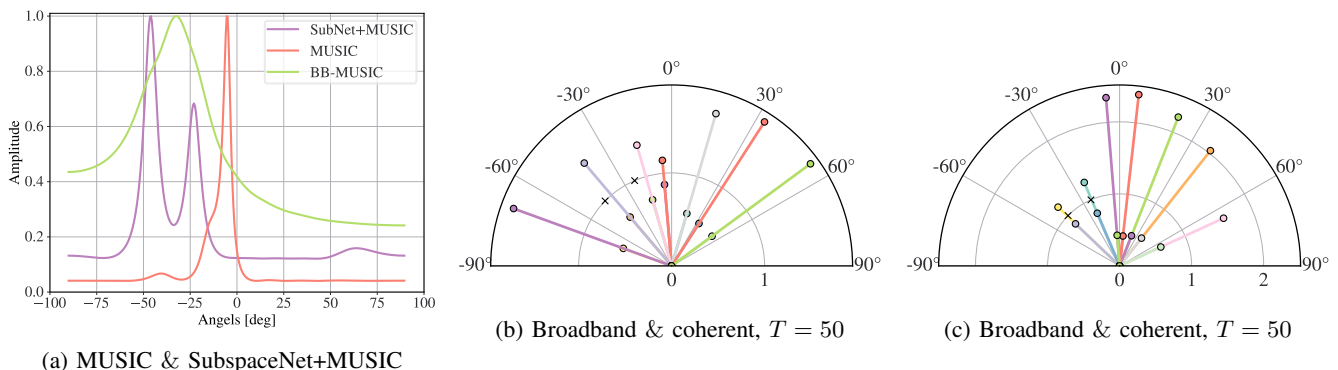


Fig. 12: Spectrum representation: $M = 3$ Wide-band coherent sources

which enhances the effectiveness of beamforming for signals with both broadband and coherent characteristics.

V. CONCLUSIONS

We proposed SubspaceNet, which enables subspace-based DoA estimation in challenging settings where a reliable division of the array input into signal and noise subspaces is typically infeasible. SubspaceNet is designed by augmenting subspace methods with deep learning tools, and it is particularly trained to produce a surrogate covariance that is universally useful for subspace-based DoA estimation by identifying Root-MUSIC as a suitable differentiable method and converting it into a trainable architecture. SubspaceNet leverages data to learn to divide the observations into signal and noise subspaces. Our results demonstrate its ability to successfully cope with coherent sources, broadband signals,

few snapshots, low SNR, and array miscalibrations, while preserving the interpretability of model-based subspace methods, and facilitating the operation of other covariance-based algorithms such as MVDR.

REFERENCES

- [1] D. H. Shmuel, J. P. Merkofer, G. Revach, R. J. G. van Sloun, and N. Shlezinger, "Deep root MUSIC algorithm for data-driven DoA estimation," in *IEEE International Conference on Acoustics, Speech and Signal Processing (ICASSP)*, 2023.
- [2] J. Benesty, I. Cohen, and J. Chen, *Fundamentals of signal enhancement and array signal processing*. John Wiley & Sons, 2017.
- [3] R. Schmidt, "Multiple emitter location and signal parameter estimation," *IEEE Trans. Antennas Propag.*, vol. 34, no. 3, pp. 276–280, 1986.
- [4] A. J. Barabell, "Improving the resolution performance of eigenstructure-based direction-finding algorithms," in *IEEE International Conference on Acoustics, Speech and Signal Processing (ICASSP)*, 1983.

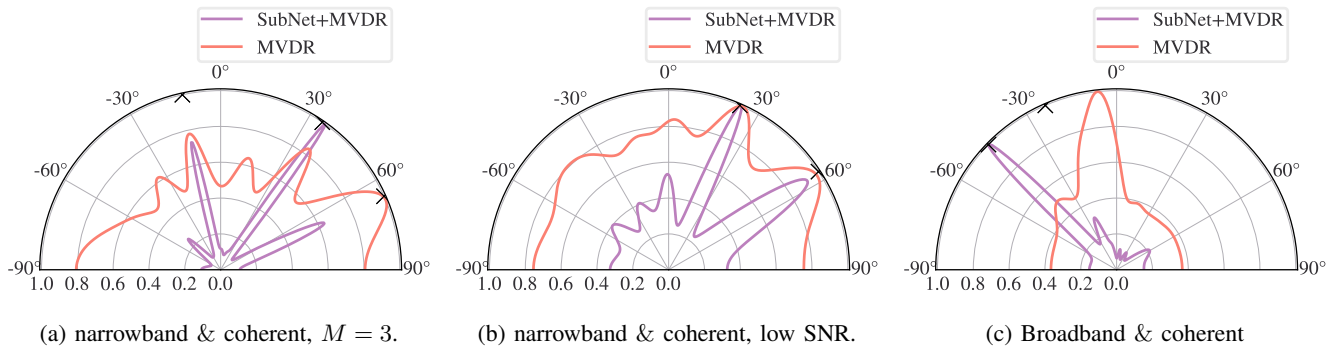


Fig. 13: SubspaceNet & MVDR beampattern comparison

- [5] R. Roy and T. Kailath, "ESPRIT-estimation of signal parameters via rotational invariance techniques," *IEEE Trans. Acoust., Speech, Signal Process.*, vol. 37, no. 7, pp. 984–995, 1989.
- [6] H. Wang, K. R. Liu, and H. Anderson, "Spatial smoothing for arrays with arbitrary geometry," in *IEEE International Conference on Acoustics, Speech and Signal Processing (ICASSP)*, 1994.
- [7] C. Qi, Y. Wang, Y. Zhang, and Y. Han, "Spatial difference smoothing for DoA estimation of coherent signals," *IEEE Signal Process. Lett.*, vol. 12, no. 11, pp. 800–802, 2005.
- [8] Y. LeCun, Y. Bengio, and G. Hinton, "Deep learning," *Nature*, vol. 521, no. 7553, p. 436, 2015.
- [9] M. Chen, Y. Gong, and X. Mao, "Deep neural network for estimation of direction of arrival with antenna array," *IEEE Access*, vol. 8, pp. 140 688–140 698, 2020.
- [10] W. Zhu and M. Zhang, "A deep learning architecture for broadband doa estimation," in *IEEE International Conference on Communication Technology (ICCT)*, 2019, pp. 244–247.
- [11] S. Chakrabarty and E. A. P. Habets, "Broadband DoA estimation using convolutional neural networks trained with noise signals," in *IEEE Workshop on Applications of Signal Processing to Audio and Acoustics (WASPAA)*, 2017, pp. 136–140.
- [12] G. K. Papageorgiou, M. Sellathurai, and Y. C. Eldar, "Deep networks for direction-of-arrival estimation in low SNR," *IEEE Trans. Signal Process.*, vol. 69, pp. 3714–3729, 2021.
- [13] L. Wu, Z.-M. Liu, and Z.-T. Huang, "Deep convolution network for direction of arrival estimation with sparse prior," *IEEE Signal Process. Lett.*, vol. 26, no. 11, pp. 1688–1692, 2019.
- [14] M. L. Lima de Oliveira and M. J. G. Bekooij, "ResNet applied for a single-snapshot DOA estimation," in *IEEE Radar Conference (Radar-Conf)*, 2022.
- [15] D. Hu, Y. Zhang, L. He, and J. Wu, "Low-complexity deep-learning-based DOA estimation for hybrid massive MIMO systems with uniform circular arrays," *IEEE Wireless Commun. Lett.*, vol. 9, no. 1, pp. 83–86, 2020.
- [16] F. Weißer, M. Baur, and W. Utschick, "Unsupervised parameter estimation using model-based decoder," *arXiv preprint arXiv:2211.01849*, 2022.
- [17] D. Chen, S. Shi, X. Gu, and B. Shim, "Robust DoA estimation using denoising autoencoder and deep neural networks," *IEEE Access*, vol. 10, pp. 52 551–52 564, 2022.
- [18] A. M. Elbir, "DeepMUSIC: Multiple signal classification via deep learning," *IEEE Sensors Letters*, vol. 4, no. 4, pp. 1–4, 2020.
- [19] C. Liu, W. Feng, H. Li, and H. Zhu, "Single snapshot DOA estimation based on spatial smoothing MUSIC and CNN," in *IEEE International Conference on Signal Processing, Communications and Computing (ICSPCC)*, 2021.
- [20] K. Lee *et al.*, "Deep learning-aided coherent direction-of-arrival estimation with the FTMR algorithm," *IEEE Trans. Signal Process.*, vol. 70, pp. 1118–1130, 2022.
- [21] J. P. Merkofer, G. Revach, N. Shlezinger, and R. J. van Sloun, "Deep augmented MUSIC algorithm for data-driven DoA estimation," in *IEEE International Conference on Acoustics, Speech and Signal Processing (ICASSP)*, 2022, pp. 3598–3602.
- [22] H. Al Kassir, Z. D. Zaharis, P. I. Lazaridis, N. V. Kantartzis, T. V. Yioultis, and T. D. Xenos, "A review of the state of the art and future challenges of deep learning-based beamforming," *IEEE Access*, 2022.
- [23] N. Shlezinger, J. Whang, Y. C. Eldar, and A. G. Dimakis, "Model-based deep learning," *Proc. IEEE*, vol. 111, no. 5, pp. 465–499, 2023.
- [24] N. Shlezinger, Y. C. Eldar, and S. P. Boyd, "Model-based deep learning: On the intersection of deep learning and optimization," *IEEE Access*, vol. 10, pp. 115 384–115 398, 2022.
- [25] N. Shlezinger and T. Rountenberg, "Discriminative and generative learning for linear estimation of random signals [lecture notes]," *IEEE Signal Process. Mag.*, 2023, early access.
- [26] L. C. Godara, *Smart antennas*. CRC press, 2004.
- [27] Y.-S. Yoon, L. M. Kaplan, and J. H. McClellan, "TOPS: new DOA estimator for wideband signals," *IEEE Trans. Signal Process.*, vol. 54, no. 6, pp. 1977–1989, 2006.
- [28] P. Stoica, R. L. Moses *et al.*, *Spectral analysis of signals*. Pearson Prentice Hall Upper Saddle River, NJ, 2005, vol. 452.
- [29] I. Goodfellow, Y. Bengio, and A. Courville, *Deep Learning*. MIT Press, 2016, <http://www.deeplearningbook.org>.
- [30] B. Luijten, R. Cohen, F. J. de Bruijn, H. A. W. Schmeitz, M. Mischi, Y. C. Eldar, and R. J. G. van Sloun, "Adaptive ultrasound beamforming using deep learning," *IEEE Trans. Med. Imag.*, vol. 39, no. 12, pp. 3967–3978, 2020.
- [31] T. Rountenberg and J. Tabrikian, "Bayesian parameter estimation using periodic cost functions," *IEEE Trans. Signal Process.*, vol. 60, no. 3, pp. 1229–1240, 2012.
- [32] J. Bolte, T. Le, E. Pauwels, and T. Silveti-Falls, "Nonsmooth implicit differentiation for machine-learning and optimization," *Advances in neural information processing systems*, vol. 34, pp. 13 537–13 549, 2021.
- [33] O. Solomon, R. Cohen, Y. Zhang, Y. Yang, Q. He, J. Luo, R. J. van Sloun, and Y. C. Eldar, "Deep unfolded robust PCA with application to clutter suppression in ultrasound," *IEEE Trans. Med. Imag.*, 2019.
- [34] A. Paszke, S. Gross, S. Chintala, G. Chanan, E. Yang, Z. DeVito, Z. Lin, A. Desmaison, L. Antiga, and A. Lerer, "Automatic differentiation in PyTorch," 2017.
- [35] J. Capon, "High-resolution frequency-wavenumber spectrum analysis," *Proc. IEEE*, vol. 57, no. 8, pp. 1408–1418, 1969.
- [36] F.-J. Chen, S. Kwong, and C.-W. Kok, "ESPRIT-like two-dimensional DOA estimation for coherent signals," *IEEE Trans. Aerosp. Electron. Syst.*, vol. 46, no. 3, pp. 1477–1484, 2010.
- [37] J.-J. Fuchs, "On the application of the global matched filter to DOA estimation with uniform circular arrays," *IEEE Trans. Signal Process.*, vol. 49, no. 4, pp. 702–709, 2001.
- [38] M. Guo, Y. D. Zhang, and T. Chen, "DOA estimation using compressed sparse array," *IEEE Trans. Signal Process.*, vol. 66, no. 15, pp. 4133–4146, 2018.
- [39] D. P. Kingma and J. Ba, "Adam: A method for stochastic optimization," *arXiv preprint arXiv:1412.6980*, 2014.